Krypton Spectroscopy Diagnosis of High-Temperature Implosions

High-temperature implosions are planned for the OMEGA Upgrade experimental program. By using relatively thin shell targets, temperatures much higher than 1 keV at modest compressed densities (~1 to 5 g/cm^3) are predicted. The goal of this work is to demonstrate that by adding a small admixture of krypton gas (~0.01 atm) to the fuel, the temperature can be conveniently diagnosed through the spectrum of helium-like (Kr^{+34}) and hydrogen-like (Kr^{+35}) lines. By increasing the fill pressure, resonant Kr lines can become opaque, through self-absorption, and their relative intensities can be used to diagnose shell-fuel mixing.

As an example of predicted high-temperature implosion on the OMEGA Upgrade system, in Fig. 61.1 we show temperature and density profiles, at peak compression, calculated by the *LILAC* code for a CH shell of 1-mm diameter and 10-μm thickness, filled with a 10-atm pressure of DT. Typical Upgrade laser parameters (laser energy of 30 kJ in a Gaussian pulse of 650-ps width) were assumed. As Fig. 61.1 shows, the core temperature and density are fairly uniform at ~5 keV and ~4.5 g/cm^3, respectively. In the analysis that follows, the core profiles will be assumed to be uniform as well. The relatively high temperature of the shell is expected to play an important role in transmitting core radiation.

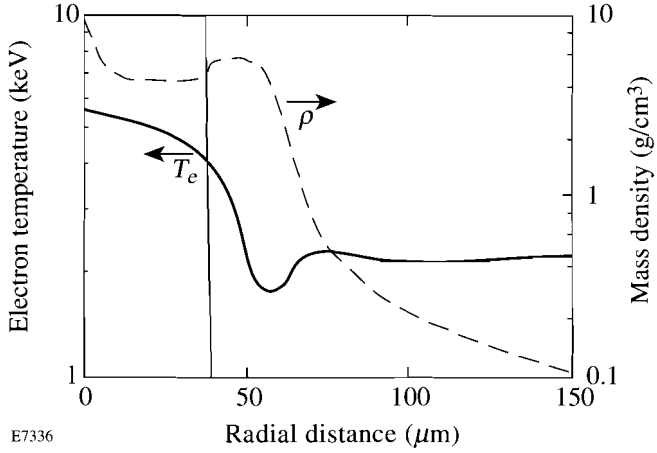

Figure 61.1
Electron temperature and mass density at peak compression, predicted by *LILAC*, for a DT-filled, high-temperature implosion on the OMEGA Upgrade system. The vertical line marks the fuel-shell interface.

Observation of K-Shell Krypton Lines

The wavelengths and transition probabilities of Kr lines are not fully known from the literature. We have used atomic data calculated by M. Klapisch,[1] using a detailed relativistic atomic structure code that includes intermediate coupling, higher-multipole interactions, and many-body and QED effects. The K-shell lines are of much shorter wavelength than past spectral line emission from laser targets; for example, the Kr^{+34} resonance line has a wavelength[1] of 0.94538 Å, or photon energy of 13.11347 keV. For this reason, we addressed the question of observability of these lines. A simple way to estimate the expected intensity of krypton lines is to make a comparison with past experiments on argon-filled targets. In recent experiments on OMEGA, strong helium-like and hydrogen-like argon lines were observed when the argon fill pressure was 0.1 atm (in 20-atm deuterium).[2] In other experiments the argon fill pressure was as low as 0.01 atm but still yielded significant spectral intensity. We chose to calculate the intensity of K-shell krypton lines using the corona approximation. This approximation was used to show only the intensity scaling; for the temperature-determination curves, the more general collisional-radiative model was used. The corona approximation is valid in the limit of low density, high temperature, and high nuclear charge Z, while the converse is true for the LTE approximation. The condition for the applicability of the corona model to excited states can be written as [Eq. (6-55) in Ref. 3]

$$N_e\left(\mathrm{cm}^{-3}\right) \ll 10^{18}\left(Z^7/n^{17/2}\right)\left(kT/E_i\right)^{1/2}, \qquad (1)$$

where E_i is the ionization energy and n is the highest principal quantum number for which the model applies. For helium-like krypton (of energy of ionization[4] E_i = 17.296 keV) and the predicted densities of up to $N_e \sim 10^{24}$ cm^{-3} ($\rho \sim 4$ g/cm^3), the model applies to quantum numbers n of up to at least $n = 3$, over the entire 1- to 10-keV temperature range. In the corona

approximation, the line intensity is given by the rate of excitation by electron collisions:[5]

$$I_\nu = h\nu\langle\sigma_{\text{exc}}v\rangle N_i N_e$$
$$= 1.6\times10^{-5} f\langle g\rangle N_e\left[\Delta E(kT)^{1/2}\right]^{-1}\exp\left[-(\Delta E/kT)\right], \qquad (2)$$

where ΔE is the excitation energy, N_i and N_e are the densities of emitting ions and electrons, respectively, f is the absorption oscillator strength, and $\langle g\rangle$ is the Maxwellian-averaged Gaunt factor[5] (kT and ΔE are in eV). Thus, if the ratio $\Delta E/kT$ is maintained when krypton is used instead of argon, the intensity of the same transition should drop by a factor of ~8 since ΔE increases by a factor of 4. The actual drop in intensity would be much smaller for the following reasons: (a) For argon, Eq. (2) would yield an overestimate of the intensity since in the corona approximation every excitation leads to a photon emission, while for argon some of the excitations result in super-elastic collisions with free electrons; (b) whereas the predicted compressed density is comparable to what was achieved with argon, the krypton targets will be bigger and thus contain more mass (by a factor of ~64) for the same fill pressure. This leads to the conclusion that the strong K-shell krypton lines will be readily observable for temperatures ≥ 3 keV.

Supportive evidence can be found in the fact that the resonance line of Kr^{+34} (at 0.94538 Å) was easily observable on previous short-pulse (100-ps) experiments[6] on OMEGA, using a Von-Hamos focusing spectrometer. The peak laser power in those experiments was ~6 TW, which is much lower than that of the OMEGA Upgrade (~30 TW).

Determination of Temperature by Line-Intensity Ratio

We now calculate the temperature dependence of a particular Kr line-intensity ratio under steady-state conditions, using the collisional-radiative atomic code POPION.[7] Although the corona model is largely applicable for the cases under discussion, as was mentioned previously, the collisional-radiative model is more precise. For example, we examined the calculated relative specie and level populations for Kr^{+34} and Kr^{+35} ions. In Fig. 61.2 we show examples of level populations in Kr^{+34} (helium-like krypton); the sum of populations in all levels of krypton ions adds up to 1. The ground-level population (especially at the higher temperatures) is essentially independent of the electron density N_e, which is a characteristic of the corona model [see Eq. (6-95) in Ref. 3]. At lower temperatures, the relative ground-level population approaches an inverse dependence on N_e, which in turn is a characteristic of the LTE model [as can be seen from the Saha equation, Eq. (6-29) in Ref. 3]. Also, the $n = 2$ population increases like N_e—also a characteristic of the corona model. The latter can be seen from Eq. (2), by equating I_ν with $h\nu\, N_i\, Q_n$, where Q_n is the relative level population in the level n. On the other hand, at the lower temperatures the $n = 2$ level population approaches independence of N_e, a characteristic of the LTE model (where relative level populations depend only on the temperature, through the Boltzmann factors). Thus, to cover the whole relevant parameter space, a full collisional-radiative model is necessary.

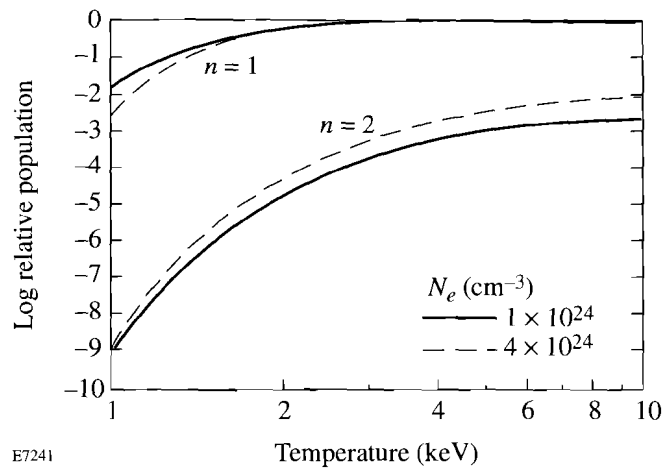

Figure 61.2
Relative populations in levels of Kr^{+34} (helium-like krypton), as calculated by the POPION[7] atomic code. The sum of populations in all levels of krypton ions adds up to 1.

For a temperature-sensitive line-intensity ratio we choose the ratio of a hydrogen-like line to a helium-like line. To minimize opacity effects we use the following two lines: (a) the Lyman-α line of Kr^{+35} of wavelength 0.9196 Å,[8] and (b) the helium-β line of Kr^{+34} of wavelength 0.8033 Å and absorption oscillator strength 0.1293.[1] We must show that the opacity of these lines will be negligible for the method to be applicable. We concentrate on the helium-β line since the opacity of the Lyman-α line is much smaller. The line opacity at an energy separation δE from the unperturbed position can be expressed as [see Eq. (8-14) in Ref. 3]

$$\tau(\delta E = 0) = \left(\pi e^2 h/Mmc\right)P(\delta E = 0) f\, \rho R\, \varepsilon Q_n, \qquad (3)$$

where M is the krypton ionic mass, $P(\delta E)$ is the line profile at δE in inverse energy units, f is the absorption oscillator

strength of the line, ρR is the total areal density (mostly that of the fuel), ε is the fraction of krypton in the fuel (by mass), and Q_n is the fraction of krypton ions in the absorbing level (i.e., the lower level of the transition). For unshifted lines one usually calculates $\tau_0 = \tau(\delta E = 0)$, but for the helium-$\beta$ line, which is shifted by the Stark effect, we designate τ_0 as the maximum opacity at the shifted peak position. In either case, $P(0) \sim 1/\Delta E$, where ΔE is the line width. We assume the addition of 0.01 atm krypton to the DT-filled target implosion that was simulated in Fig. 61.1. In that implosion the DT fill pressure was 10 atm, and the total ρR at peak compression was ~16 mg/cm^2. According to the POPION code results (Fig. 61.2), Q_1 for helium-like Kr over a wide temperature range is very close to 1.

Next we need to estimate the line width, which is related to $P(0)$ in Eq. (3) as explained previously. The code results of Fig. 61.1 show that the ion temperature at peak compression is about twice the electron temperature, or $T_i \sim 10$ keV, for which the Doppler width of the helium-β line is about 12.9 eV. A rough estimate of the Stark width of the Kr^{+34} helium-β line can be obtained by noting that for a given density and temperature the Stark width is proportional to $1/Z$. More specifically, the scaling for the Stark width of hydrogenic lines is[11] given by $\Delta E \sim \left(Z_p/Z\right)\left(n_i^2 - n_f^2\right)N_p^{2/3}$, where Z_p and N_p are respectively the nuclear charge and ion density of the perturber, Z is the nuclear charge of the emitter, and n_i, n_f are the principal quantum numbers of the initial and final levels of the transition. Although the ion under discussion is helium-like, the Stark width of the upper level, $1s3p\,^1P$, turns out to exceed the separation to the nearby $1s3d\,^1D$ level, which makes the transition close to hydrogenic (i.e., the level splitting increases linearly with the perturbing field as in single-electron ions). The above formula for the Stark width is only approximate and does not include such effects as perturbers correlation. However, we use its Z scaling only for extrapolating the detailed calculations[10] for the same transition in argon at the same density and ignore the weak temperature dependence of the Stark broadening. The Stark width of the Kr^{+34} helium-β line at $\rho = 4.5$ g/cm^3 is thus estimated to be ~17 eV. Convolving this Stark width with the Doppler width yields a total width of ~26 eV, from which the normalized composite profile yields the value of $P(\delta E)$. Substituting these values into Eq. (3) yields an optical depth for the helium-β line of $\tau_0 \sim 0.56$. This opacity value was estimated for an electron temperature of 5 keV ($T_i \sim 2\,T_e$) and density of 4.5 g/cm^3. For other temperatures (but the same doping fraction) the opacity will not change appreciably because (1) Q_1 is weakly dependent on T in the range T_e ~3 to 10 keV (see Fig. 61.2), and (2) the linewidth depends mainly on the density. For other densities the opacity will vary as $\sim\rho^{-2/3}$ due to the change in linewidth. The opacity of the Lyman-α line of Kr^{+35} is much smaller than that of the helium-β line because the ratio of Kr^{+35} to Kr^{+34} ground-state populations at $N_e = 10^{24}$ cm^{-3} varies over the 1- to 10-keV temperature range from $\sim 10^{-10}$ to $\sim 10^{-1}$.

The curves in Fig. 61.2 and the temperature curves calculated below assume a steady-state situation. To justify this assumption we show in Fig. 61.3 the calculated ionization time t_i of the Kr^{+34} ion as a function of temperature for $N_e = 10^{24}$ cm^{-3}; t_i depends inversely on N_e and is given by $t_i = \left(\langle\sigma_{\text{ion}}v\rangle N_e\right)^{-1}$. The ionization rate was taken as[11]

$$\langle\sigma_{\text{ion}}\rangle = 2.5\times10^{-6}\,\eta\,E_i^{-3/2}\left(kt/E_i\right) \times \left[1+\left(kT/E_i\right)\right]^{-1}\exp\left[-\left(E_i/kT\right)\right], \quad (4)$$

where E_i is the ionization energy (in eV) and η is the number of outer-shell electrons ($\eta = 2$ for helium-like ions). The time constant for approaching a steady state of level populations for a given set of hydrodynamic conditions is given by t_i since t_i is the slowest of the relevant processes. An example can be found in the excitation rate from the ground level to the 2^1P level of Kr^{+34}, which is faster than the ionization rate by a factor that varies from ~700 at the low end of the temperature range to ~3 at the higher end. We see from Fig. 61.3 that for a value of T of 5 keV, the ionization time t_i is ~50 ps, which is about the time period t_{peak} predicted for the volume-averaged temperature to be within ~90% of its peak value. Thus, the

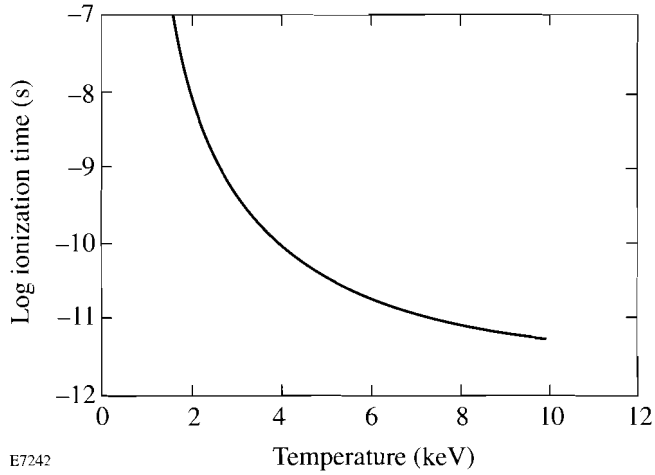

Figure 61.3
Calculated ionization time t_i of Kr^{+34} as a function of temperature, for $N_e = 10^{24}$ cm^{-3}. The ionization time serves as a time constant for approaching a steady state of level populations for a given set of hydrodynamic conditions.

density of hydrogen-like ions will reach only the fraction $\left[1-\exp\left(-t_{\text{peak}}/t_i\right)\right] \sim 0.63$ of its steady-state value. Neglecting this effect will result in an underestimate of the temperature (in the above example, 4.6 keV instead of 5 keV). An underestimate will also result if the spectral measurement is not time resolved, since the emission time of helium-like lines will be longer than that of hydrogen-like lines.

We show in Fig. 61.4 the calculated intensity ratio of the Lyman-α line of Kr^{+35} to the helium-β line of Kr^{+35} as a function of temperature for two electron-density values. Clearly, the intensity-ratio change is sensitive to temperature, but the Lyman-α line may be too weak to be observed for temperatures smaller than ~4 keV. In going from $T = 10$ keV to $T = 4$ keV, both the ratio in Fig. 61.4 and the intensity of the helium-β line drop by an order of magnitude, which causes the intensity of the Lyman-α line to drop by two orders of magnitude. Over a wide density range (changing by a factor of 20), the temperature-dependence curve changes very little. This behavior is due to the close resemblance to the corona model, where the line ratio is completely independent of density. If we know the density to be within this range, the maximum error in determining the temperature would be less than ±10%. The required precision in the intensity measurements is modest: to achieve a ±10% precision in the temperature, the intensity ratio must be measured with a precision of only a factor of ~3 (at $T = 4$ keV) or a factor of ~2 (at $T = 6$ keV). The attenuation of these two lines through the compressed CH polymer shell is of no concern, as a cold $\rho\Delta R$ of more than 1 g/cm^2 is needed to significantly attenuate them.

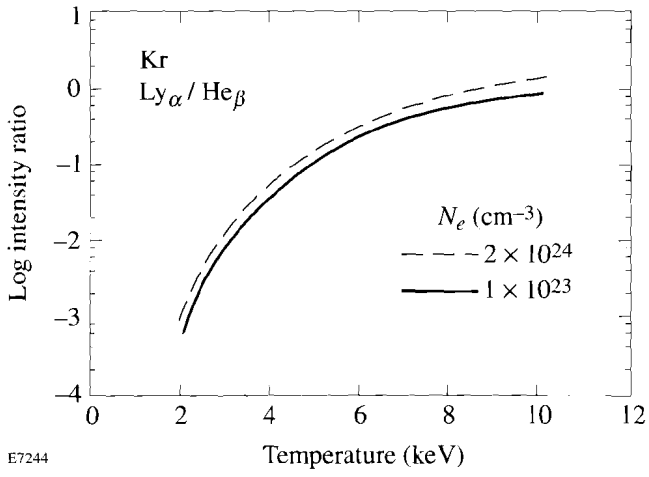

Figure 61.4
Intensity ratio of the Lyman-α line of Kr^{+35} to the helium-β line of Kr^{-35} as a function of temperature at two electron-density values. The opacity of both lines, which was shown to be small, was neglected.

Mixing Diagnosis Based on High-Opacity Kr Lines

In the previous section the opacity of the helium-β line of Kr^{+34} for a fill pressure of 0.01 atm was shown to be smaller than 1 ($\tau_0 \sim 0.56$), and thus negligible. We now examine the case of much higher fill pressures, where the helium-β line is optically thick at peak compression. Although the intensity ratio in Fig. 61.4 is then not applicable, a different type of information can be obtained on the target behavior. Anticipating the last section, we choose the helium-β line rather than the higher-opacity helium-α line.

The intensity of an optically thick line emerging from the plasma volume is related to the escape factor parameter, which has been the subject of numerous publications.[12–15] The escape factor G is defined by

$$G(\tau_0) = \int_{-\infty}^{\infty} P(\delta E)\exp\left[-\tau_0 P(\delta E)/P(\delta E = 0)\right] d(\delta E), \quad (5)$$

where $G(\tau_0)$ in spherical geometry corresponds to a point source at the center of the sphere and τ_0 is the opacity over the radius. For a source uniformly distributed over the sphere, Mancini *et al.*[15] have shown that $G(\tau_0)$ is twice as big as the point-source case and depends primarily on the type of line profile. For example, for a Gaussian (i.e., Doppler) profile, $G(\tau_0)$ does not depend explicitly on the linewidth; for $\tau_0 >> 1$, $G(\tau_0) \sim 1/\left(\pi \ln \tau_0\right)^{1/2} \tau_0$. For Stark profiles the corresponding asymptotic relation was found to be $G(\tau_0) \sim 1/\tau_0^{3/5}$. For example, a Holtzmarkian profile (the simplest approximation to a Stark profile) yields the universal asymptotic expression[12]

$$G(\tau_0) = 0.451/\tau_0^{3/5} \qquad (\tau_0 >> 1). \quad (6)$$

Mancini *et al.*[15] have calculated $G(\tau_0)$ for the Lyman-α line of argon using complete Stark profiles. They showed that for an accurate value of G, a detailed calculation with an actual Stark profile should be performed. However, their curves (for a point source) can still be approximated by Eq. (6) if G is expressed as a function of τ_0, rather than as a function of $\tau_0/P(\delta E = 0)$, because an approximate Stark profile that changes only the line width without changing the profile shape will not affect Eq. (6).

A measurement of the escape factor of a high-opacity line can yield the value of τ_0, using Eq. (6) or the equivalent result of a more detailed calculation.[15] As Eq. (3) shows, τ_0 depends on ρR and, through $P(\delta E)$, on ρ. For a high-opacity line, most of the emergent intensity is located in the far wings of the

spectral profile. Because the Doppler profile drops much faster than the Stark profile, the wings are dominated by the latter, although the two separate linewidths are comparable. For this reason we consider the escape factor for a purely Stark profile. For the helium-β line, $P_0 = P(\delta E = 0) \sim \rho^{-2/3}$, when the density is high enough to merge the $1s3p$ and $1s3d$ levels, which we have argued to be the case here. For the crude estimate of 17-eV Stark width, this relationship reads

$$P_0\left(\mathrm{eV}^{-1}\right) = 0.15\,\rho^{-2/3}, \tag{7}$$

where, as explained, P_0 refers to the peak of the profile rather than to the line center. On the other hand, in an imploding spherical target

$$\rho R = \left(3M_F/4\pi\right)^{1/3}\rho^{2/3} \tag{8}$$

in terms of the total fill mass (fuel and krypton) M_F. Thus τ_0 is independent of the target compression because the opacity increases with increasing ρR but decreases due to the increasing width (or decreasing P_0). The two quantities change as $\rho^{2/3}$ and cancel each other's effect on τ_0.

The foregoing discussion shows that measuring the escape factor cannot yield information on the density or ρR. Mixing of shell material into the fuel, however, does affect the escape factor measurement because the ρR deduced from the absorption of Kr lines yields the ρR of only the fuel $(\rho R)_F$, whereas the Stark profile depends on the total density ρ_T, including shell material mixed into the fuel. Combining Eqs. (3), (7), and (8), we can relate the volume-averaged fraction of density due to mixing $\xi = \rho_{\mathrm{mix}}/\rho_F$ to τ_0:

$$1 + \xi = \left[0.15\,\pi e^2 h\, f\left(eM_F/4\pi\right)/\left(mMc\,\tau_0\right)\right]^{3/2}. \tag{9}$$

We can understand the effect of mixing on the opacity as follows: Without mixing, the opacity τ_0 is approximately constant during the compression because of the two opposing effects: (1) increase in the ρR of absorbing ions and (2) increase in the linewidth. The mixed shell material is involved only in the second effect, which causes a net reduction in the opacity.

The experimental determination of the mixing fraction consists of measuring the escape factor $G(\tau_0)$, deducing τ_0 from Eq. (6) (or from a more detailed equivalent thereof), and, finally, finding ξ from Eq. (9). In addition to using a crude Stark profile, Eq. (9) is correct only for a point source (central hot spot). As mentioned earlier, Mancini *et al.*[15] have shown that for a spherically uniform source, $G(\tau_0)$ is twice as big as for the point-source case. To determine which geometry conforms better to the experiment we can examine two experimental signatures: (a) for a uniform source, the core image size at high photon energy will be about the same as that at low photon energy, whereas for a hot-spot source the former will be much smaller than the latter; and (b) for a uniform source the observed line profile will be flat topped, whereas for a hot-spot source a self-reversal (or minimum) will be observed at the position of the profile peaks.

A Method for Measuring the Escape Factor

The escape factor of a line can be measured by comparing its measured intensity to that of another line, both of which have the same upper level. The first should have an opacity $\tau_0 >> 1$, the second $\tau_0 << 1$. The two helium-like Kr lines we selected are (a) the Lyman-β line, $1s3p\,^1P - 1s^2\,^1S$ (at 0.8033 Å) and (b) the Balmer-α line, $1s3p\,^1P - 1s2s\,^1S$ (at 5.0508 Å). Note that what we refer to here as Balmer-α is the helium-like, 3-2 transition that shares an upper level with the helium-β line (and not, for example, to the stronger $1s3d\,^1D - 1s2p\,^1P$ transition at 5.3463 Å). Previously, we mentioned the helium-α line corresponding to the $1s2p\,^1P - 1s^2\,^1S$ transition. For krypton ions, both the transitions to the ground level and the 3-2 transitions are easily accessible to x-ray measurement. Thus, for argon, the 3-2 transitions are too soft ($\lambda > 20$ Å) for common x-ray crystal instruments, and they also suffer very high opacity in traversing the target.

By making an appropriate choice of the krypton fill pressure, the opacity (for resonant absorption) of the Lyman-β line at peak compression will be >>1, while that of the Balmer-α will be <<1. It was estimated earlier that for a Kr fill pressure of 0.01 atm, the opacity τ_0 of the helium-β line will be ~0.5. Thus, for a fill pressure in the range of 0.1 to 1.0 atm, τ_0 will be in the range of 5 to 50. The opacity of the Balmer-α line will still be negligible since it is absorbed by ions in the $n = 2$ shell (whereas the helium-β line is absorbed by ground-level ions). Figure 61.2 shows that the population of $n = 2$ absorbing ions is smaller than that of $n = 1$ absorbing ions by several orders of magnitude. Due to the expected merging of the $1s3p\,^1P$ and $1s3d\,^1D$ levels, both ions in the $1s2p\,^1P$ and $1s2p\,^1S$ levels can absorb the broadened Balmer-α line; these constitute 1/3 of all $n = 2$ ions. With no merging, only 1/16 of the $n = 2$ ions can absorb the $1s3p\,^1P - 1s2s\,^1S$ transition. The high opacity of the resonance line $1s^2 - 1s2p\,^1P$

will also increase the $n = 2$ population (this effect is not included in Fig. 61.2).

In the absence of any absorption, the intensity ratio of these two lines I_{Ly}/I_{Ba} would simply be given by the ratio of the Einstein A coefficients (spontaneous emission probabilities) A_{Ly}/A_{Ba} and be independent of any atomic modeling. Since A (Lyman-β) = 4.453×10^{14} s^{-1} and A (Balmer-α) = 6.163×10^{12} s^{-1}, $A_{Ly}/A_{Ba} = 72.25$. In the case discussed here, the observed intensity ratio I_{Ly}/I_{Ba} will be lower than the ratio of the Einstein A coefficients A_{Ly}/A_{Ba}, by the escape factor G for the helium-β line. Thus, G can be found from

$$G = \left(I_{Ly}/I_{Ba}\right)/\left(A_{Ly}/A_{Ba}\right) = \left(I_{Ly}/I_{Ba}\right)/72.25. \quad (10)$$

It should be noted that the emergent intensity of a high-opacity line may not depend uniquely on the escape factor because of the possibility of re-emission of absorbed photons.[16] This is equivalent to allowing for the increased excited-level population (and thus emission) due to the absorption itself. In our case this effect is already included in the ratio of line intensity because the measured intensity of the optically thin Balmer-α line does reflect the actual excited-level population.

The nonresonant absorption by the target material (mostly the shell) should be negligibly small to insure the validity of this method. The attenuation of the Lyman-β line through the shell is negligible: it takes a $\rho\Delta R$ of ~1.8 g/cm^2 of cold CH to attenuate that line by $1/e$. On the other hand, the Balmer-α line will be attenuated by the same amount in going through only a $\rho\Delta R$ of ~5.5 mg/cm^2 of cold CH. Figure 61.1 shows that the shell at peak compression is hot enough to minimize this attenuation. The opacity of the CH shell at a wavelength λ, due to inverse bremsstrahlung absorption, is given by[17] $\tau = 2.23 \times 10^{-3} \lambda^3 (\rho\Delta R)\rho/T^{1/2}$, where λ is in Å and T in keV. For the target profiles of Fig. 61.1, the inverse bremsstrahlung opacity is $\tau \sim 0.014$. The opacity of CH due to photoionization is given by[17] $\tau = 0.54\ \lambda^3(\rho\Delta R)\Psi$, where Ψ is the fraction of carbon ions that are not stripped. Results from POPION calculations show that, at the given shell temperature and density values, $\Psi < 10^{-3}$ so that the photoionization opacity is $\tau < 10^{-3}$.

Finally we estimate the expected sensitivity of the method for measuring the degree of shell-fuel mixing. To find G from Eq. (10) with a precision of approximately ±20%, the relative intensity of each of the lines must be measured with a precision of ±10%, which requires the relative calibration of two instruments for the two very different wavelengths used here. A suitable procedure is as follows: the intensity ratio I_{Ly}/I_{Ba} for the case of a very low Kr fill pressure (~0.01 atm) is simply given by the known ratio A_{Ly}/A_{Ba}. Since, for Stark profiles, G depends[15] asymptotically on τ_0 like $1/\tau_0^{3/5}$, an error of ±20% in G will result in an error of ±33% in τ_0. Finally, finding the relative mixing from Eq. (9), this error translates into an error of ±50% in $1 + \xi$. Thus, the method is useful only for extensive mixing, where ξ is not much smaller than 1.

ACKNOWLEDGMENT

This work was supported by the U.S. Department of Energy Office of Inertial Confinement Fusion under Cooperative Agreement No. DE-FC03-92SF19460, the University of Rochester, and the New York State Energy Research and Development Authority. The support of DOE does not constitute an endorsement by DOE of the views expressed in this article.

REFERENCES

1. M. Klapisch (private communication).
2. B. Yaakobi, R. Epstein, F. J. Marshall, D. K. Bradley, P. A. Jaanimagi, and Q. Su, Optics Commun. **111**, 556 (1994).
3. H. R. Griem, *Plasma Spectroscopy* (McGraw-Hill, New York, 1964).
4. U. I. Safranova, Physica Scripta **23**, 241 (1981).
5. H. Van Regemorter, Astrophys. J. **136**, 906 (1962).
6. B. Yaakobi and A. J. Burek, IEEE J. Quantum Electron. **QE-19**, 1841 (1983).
7. R. Epstein, S. Skupsky, and J. Delettrez, J. Quant. Spectrosc. Radiat. Transfer **35**, 131 (1986).
8. G. W. Ericson, J. Phys. Chem. Ref. Data **6**, 831 (1977).
9. H. R. Griem, *Spectral Line Broadening by Plasmas* (Academic Press, New York, 1974).
10. C. F. Hooper (private communication).
11. H.-J. Kunze, A. H. Gabriel, and H. R. Griem, Phys. Rev. **165**, 267 (1968).
12. F. E. Irons, J. Quant. Spectrosc. Radiat. Transfer **22**, 1 (1979).

13. J. P. Apruzese, *ibid.* **34,** 447 (1985).

14. C. Chenais-Popovics, P. Alaterre, P. Audebert, J. P. Geindre, and J. C. Gauthier, *ibid.* **36**, 355 (1986).

15. R. C. Mancini, R. F. Joyce, and C. F. Hooper, Jr., J. Phys. B: At. Mol. Phys. **20**, 2975 (1987).

16. A. G. Hearn, Proc. Phys. Soc. (GB) **81**, 648 (1963).

17. B. Yaakobi, R. Epstein, and F. J. Marshall, Phys. Rev. A **44**, 8429 (1991).